THE ASTROPHYSICAL JOURNAL, 415:129–139, 1993 September 20

THE *ROSAT* SPECTRUM OF 3C 351: A WARM ABSORBER IN AN X-RAY–"QUIET" QUASAR?

FABRIZIO FIORE, MARTIN ELVIS, SMITA MATHUR, BELINDA J. WILKES, AND JONATHAN C. MCDOWELL
Harvard-Smithsonian Center for Astrophysics, 60 Garden Street, Cambridge, MA 02138
Received 1992 December 15; accepted 1993 March 25

ABSTRACT

3C 351 is one of the most X-ray–quiet radio quasars ($\alpha_{ox} \sim 1.6$). We have observed 3C 351 with the *ROSAT* position sensitive proportional counter (PSPC) and find a complex X-ray spectrum which is not well reproduced by a power law plus low-energy cutoff model. Soft excess, partial covering, and "warm absorber" models can all produce acceptable fits, although only the warm absorber model gives typical values for the high-energy continuum slope. The α_{ox} measured by using quasi-simultaneous *ROSAT*, MMT, and *HST* observations is in the range 1.5–1.6, significantly above the average of 1.37 ($\sigma \sim 0.15$) for a complete sample of 33 3CR quasars. If the soft excess or partial covering models are correct, 3C 351 appears X-ray–quiet in the PSPC band because it has an extremely steep or flat intrinsic high-energy spectral slope. However, if the warm absorber model is correct, the quasar is intrinsically X-ray–quiet; the normalization of the intrinsic (unabsorbed) X-ray emission is unusually low relative to the optical luminosity. We investigate the properties of our warm absorber model in some detail. The apparently complicated behavior of the fit parameters may be understood by considering the effects of changing absorbing column and ionization parameter on intrinsic power-law spectra of different slopes.

Subject headings: quasars: individual (3C 351) — X-rays: galaxies

1. INTRODUCTION

Most quasars are X-ray sources, but the range of their X-ray output relative to the optical (or ultraviolet or infrared) is large, covering a range of ~400 (Zamorani et al. 1981; Tananbaum et al. 1986). While Avni & Tananbaum (1986) showed that only a minority (less than 8%) of all quasars could be "X-ray silent," they also found that most quasars are relatively X-ray–quiet. In terms of the commonly used parameter α_{ox} (the two-point spectral index between the optical [2500 Å] and X-ray [2 keV]) this distribution covers the range from $\alpha_{ox} \sim 0.9$ to $\alpha_{ox} \sim 2$ (Tananbaum et al. 1986; Elvis & Fabbiano 1984; Makino et al. 1989).

What is the cause of this "X-ray–quietness"? Extreme spectra, either flat (or absorbed) or steep, could remove photons from the observed band without affecting the X-ray flux; a low normalization to the spectra is a possibility, so that the same process is 400 times less efficient at generating X-rays in some quasars than in others; and, since observations establishing L_{opt} and L_X have not been made simultaneously, large-amplitude X-ray variability by a factor of ~400 in the few years between the optical and X-ray observations, even though variations of only a factor of ~2 are typical in the optical, could produce a range of X-ray loudness. Each of these explanations would involve extreme physics, and most imply unusual spectral properties.

X-ray quietness is less extreme among radio-loud quasars. A complete sample of 3CR quasars [$f(178\ \mathrm{MHz}) > 9$ Jy and $V < 18$] was studied in X-rays by Tananbaum et al. (1983), who detected all 33 objects. They found a maximum α_{ox} of 1.67. 3C 351 ($z = 0.371$; Véron-Cetty & Véron 1991) is one of the most X-ray–quiet radio quasars ($\alpha_{ox} = 1.6$; Tananbaum et al. 1986). It is also one of the very few X-ray–quiet quasars with an X-ray flux sufficient to obtain a spectrum with *Einstein* or *ROSAT* (1.0×10^{-12} ergs s^{-1} cm^{-2}, 0.5–4.5 keV, assuming the energy spectral index $\alpha_E = 0.5$ and Galactic absorption; Tananbaum et al. 1986). 3C 351 has a flat X-ray spectrum in the *Einstein* imaging proportional counter (IPC) (Elvis et al. 1993). On the other hand, 3C 351 qualified securely as an "ultrasoft source" in one of the 12 IPC observations (Cordova et al. 1992). Something unusual seems to be happening in the X-ray spectrum of 3C 351.

The radio structure of 3C 351 is double-lobed with most of the emission concentrated in one lobe (Leahy & Perley 1991). The total flux at 5 GHz is ~1.2 Jy and the fraction of flux density contained in the compact core is very low: 0.65% at 6 cm (Kellermann et al. 1989). In the view of unified models (Orr & Browne 1982; Barthel 1989), the dominance of the core is a measure of the inclination of the radio axis to the line of sight: core-dominated quasars are viewed with their radio axis end-on and the flux density amplified due to the Doppler effect (e.g., Blandford & Königl 1979); lobe-dominated quasars are viewed edge-on. Thus 3C 351, with its weak core, may be close to edge-on. This may be related to its X-ray quietness because the X-ray flux could be linked with the radio flux and/or because the X-ray flux could be blocked by intervening matter along the line of sight.

Before the launch of *ROSAT* (Trümper 1983) significant intrinsic absorption had been discovered only in two luminous quasars, MR 2251−178 (Halpern 1984; Pan, Stewart, & Pounds 1990) and NRAO 140 (Marscher 1988; Turner et al. 1991). In the first case the absorption is produced not by neutral gas but by partially ionized "warm" material (Halpern 1984; Pan et al. 1990). A signature of such material is a flattening of the spectrum above the oxygen K-edge at ~1 keV, and an excess flux below the edge, at ~0.25 keV, where the ionized lighter elements become transparent. There is a possibility that warm absorbers could reduce the X-ray loudness of an active galactic nucleus (AGN) without totally removing soft photons and rendering it undetectable. The *ROSAT* position sensitive proportional counter (PSPC; Pfefferman et al. 1987) bandpass (0.1–2.5 keV) is particularly useful for studying the effects of soft X-ray absorption. Furthermore, its improved

energy resolution and signal-to-noise ratio with respect to the IPC on board the *Einstein* satellite will allow the investigation of the details of such complex absorption systems.

We observed 3C 351 with the PSPC between 1991 October 28 and 30 for a total live time of 13,068 s. We find a complex X-ray spectrum which suggests that we view the quasar through a partially ionized region of gas, a warm absorber.

2. OBSERVATIONS AND DATA ANALYSIS

The distribution of the X-rays from 3C 351 was consistent with the 25″ FWHM of the PSPC point response function, and the centroid of the distribution is only 8.″7 from the optical position (R.A. $17^h04^m03^s.4$, decl. 60°48′31.″1; B1950), an offset typical of *ROSAT* pointings. Source counts were extracted from within a 2′ radius around the source centroid (containing at least 95% of the source counts; Turner & George 1992). The background was estimated within an annulus of inner and outer radii 2.′5 and 5′, respectively. Within 6′ of the 3C 351 centroid five weak sources are detected. Circular regions of radius 1.′5 centered on these sources were then excluded from the analysis. The distribution of the counts from 3C 351 falls to the background level at a radius of ~1.′5. The total net source counts within 2′ are ~1420, and the estimated background counts are ~340. During the observation, spanning over 2 days, the variations of the 0.1–2.45 keV source intensity were smaller than ≈40%, and the count rate is consistent with a value of 0.106 ± 0.003 PSPC counts s^{-1} at the 5% confidence level. Assuming $\alpha_E = 0.5$ and Galactic absorption as in Tananbaum et al. (1986), this corresponds to a 0.5–4.5 keV flux of 1.25×10^{-12} ergs s^{-1} cm^{-2}, similar to the IPC value. The 34 energy channels used by MPE SASS pipeline processing are used in the following analysis.

2.1. *Systematic Error Estimate*

The good temporal and spatial gain stability of the PSPC makes it possible to achieve a good calibration of this imaging proportional counter (*ROSAT* News, No. 10, 1992). Nevertheless, there are residual systematic uncertainties in the knowledge of the resolution matrix of the order of a few percent. In particular, the following systematic features have been found in the residuals of PSPC spectral fits of high signal-to-noise data (*ROSAT* News, No. 10, 1992): (*a*) a systematic deficiency of measured counts above the carbon edge (around 0.4 keV) with associated excesses between 0.2–0.4 keV; (*b*) an excess of measured counts about 2 keV.

To quantify the magnitude of the above systematic features, we analyzed the spectrum of the quasar PG 1426+015 (Wilkes et al. 1993), which is about 10 times brighter than 3C 351 in soft X-rays and was observed by the PSPC in 1990 July for a total live time of 6485 s and a 0.1–2.45 keV count rate of 1.4 counts s^{-1}. The pulse-height spectrum is plotted in Figure 1 along with the best-fitting power law, reduced at low energy by Galactic absorption. The fit was performed using the 1992 March version of the PSPC response matrix installed in the SASS processing system (DRM_9). The value of the reduced χ^2 (1.28 for 30 degrees of freedom [dof], corresponding to a 14% probability of finding a greater χ^2 by chance) indicates that the model is an adequate representation of the data. The best-fit values of the spectral index, the 0.1–2.45 unabsorbed flux, and the absorbing column were 1.54 ± 0.13, $(3.2 \pm 0.1) \times 10^{-11}$ ergs cm^{-2} s^{-1}, and $(2.6 \pm 0.3) \times 10^{20}$ cm^{-2} (consistent with the Galactic value of 2.64×10^{20} cm^{-2}), respectively. In the lower panels we plot the residuals after the subtraction of the model from the data both as a multiple of σ and as a fraction of the source net counts in each channel. A deficiency of the measured counts is seen around 0.4 keV (channels 10–12), as well as an excess around 0.3 keV (channels 8 and 9). The magnitude of these features is small, of the order of 1 σ per channel, or about 5% of the source net counts per channel. A small excess of the measured counts is also present above 2 keV, but in that region the statistics are not good enough to obtain useful information on the magnitude of the systematic error.

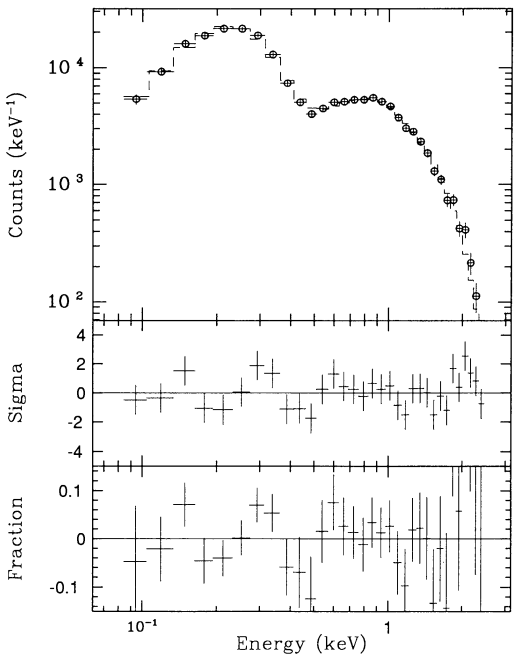

FIG. 1.—Single power law with low-energy "cold" absorption spectral fit to the spectrum of PG 1426+015. Energies are in the observed frame.

These deviations form an upper limit to the systematic errors on the PSPC response matrix, since the quasar may itself contain real spectral features more complex than a power law. The magnitude of the features is quite negligible compared with the statistical errors per channel in the spectrum of 3C 351, which range from 12% to 31% of the net source counts in those channels.

As a further test we analyzed the data of the BL Lacertae object 1E 1704.9+6047 (Gioia et al. 1990), which is in the same *ROSAT* field of 3C 351 at just 7′ from the quasar. Source counts were extracted from within 2.′5 around the source centroid, and the background was estimated within an annulus of inner and outer radii 3′ and 5.′5, respectively. The total net source counts were ~1030, comparable to those of 3C 351. The spectrum of 1E 1704.9+6047 was fitted to a simple power law plus low-energy absorption. The reduced χ^2 is 1.32 (28 dof, corresponding to a 12% probability), and the residuals do not present strong features at any energy. The column density [$N_H = (2.3 \pm 0.3) \times 10^{20}$ cm^{-2}] is compatible with the Galactic value along the line of sight of $(2.26 \pm 0.10) \times 10^{20}$ cm^{-2} (Elvis, Lockman, & Wilkes 1989). The spectral index is 1.33 ± 0.25, and the 0.1–2.45 keV unabsorbed flux is $(1.4 \pm 0.2) \times 10^{-12}$ ergs cm^{-2} s^{-1}.

In the following analysis we include a systematic error of 2% (as suggested in *ROSAT* News, No. 10, 1992) by adding it in

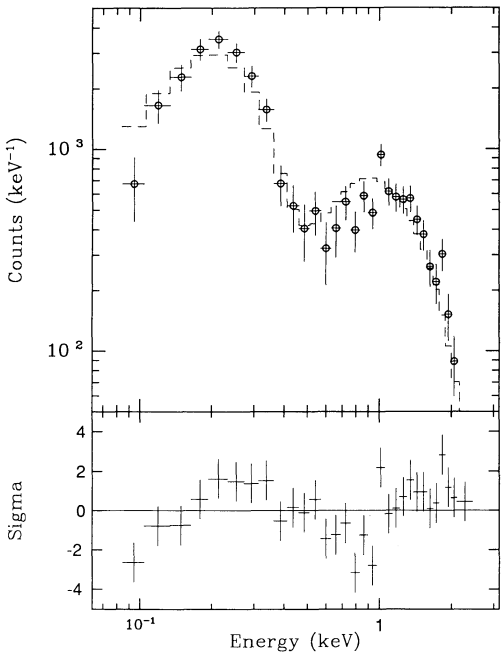

FIG. 2.—Single power law with low-energy "cold" absorption spectral fit to the spectrum of 3C 351. Energies are in the observed frame.

quadrature to the statistical error in each channel. The fits are performed over the 0.1–2.45 keV energy range (channels 2–34). The errors represent the 68% confidence interval.

3. RESULTS

3.1. *Simple Power Law*

We first attempted a fit to the 3C 351 *ROSAT* spectrum of a simple power-law model reduced at low energies by absorption from a neutral gas with solar abundance (using cross sections from Morrison & McCammon 1983; we designate this as our model 1). The results of the fit are shown in Figure 2 and given in Table 1, where the errors are given for two interesting parameters following the prescription of Lampton, Margon, & Bowyer (1976). The energy spectral index is $\alpha_E = 0.47 \pm 0.16$, rather flat for a lobe-dominated quasar and similar to that found using the *Einstein* IPC data by Elvis et al. (1993). The column density is $N_H = (0.39 \pm 0.25) \times 10^{20}$ cm^{-2}, significantly lower than the Galactic value along the line of sight of 2.26×10^{20} cm^{-2} (Elvis et al. 1989). The χ^2_r of 2.18 for 28 dof, is unacceptably large (probability of 3×10^{-4}). The poor quality of the fit is illustrated by the residuals plotted in the lower panel of Figure 2. We see a clear 36% deficit in the counts measured between 0.6 and 0.9 keV (channels 14–19); a ~15% excess between 0.2 and 0.4 keV (channels 5–9); and an excess above 1 keV. The strong deficit between 0.6 and 0.9 keV is significant at ~10 σ. This deficit cannot be explained in terms of a systematic effect in the resolution matrix, since at those energies the residuals of PG 1426+015 are flat to 5% ($\pm 1\ \sigma$; see above, Fig. 1), while the observed deficit in 3C 351 is some 2.5 times larger.[1] A fit of the same model with N_H fixed at the Galactic value gives a χ^2_r of 4.08 (29 dof), a rather steep power-law slope $\alpha_E = 1.31 \pm 0.05$, and qualitatively similar residuals. Fits with a single thermal component, such as a blackbody, a thermal bremsstrahlung, and a Raymond-Smith (1977) model, all give χ^2 significantly higher than model 1.

We must therefore investigate more complex models for 3C 351. Model 1 can be modified by changing either the emission law or the absorption law or both. We tried three modifications.

3.2. *Soft Component*

A soft component was added to the emission law, as suggested by the report of an excess in the 0.1–0.5 keV band by Cordova et al. (1992) and by the measure of an N_H much lower than the Galactic value in model 1. Parameterizing the excess as a steep power law, we obtain the results given in Table 1 and the residuals shown in Figure 3*a*. The χ^2_r is now acceptable (1.03 for 26 dof), and the improvement in its value is significant at very much more than the 99.9% confidence level, using the F-test ($F = 33.3$; a significant improvement at the 99.9% level requires $F = 13.74$; Abramowitz & Stegun 1964). The N_H of $(4.8 \pm 3.0) \times 10^{20}$ cm^{-2} is now compatible with the Galactic line-of-sight value. The spectral index of the soft power law is poorly constrained. The hard power law, however, is well determined at $\alpha_E = -0.04^{+0.34}_{-0.25}$ (errors for three interesting parameters). Such a flat spectral index is very unusual in

[1] A fit performed with the more accurate resolution matrix released in 1993 January (DRM_36_1) confirms this conclusion: the residuals appear qualitatively similar to those in Fig. 2, and the χ^2 for a simple power-law model is slightly worse than that in Table 1.

TABLE 1

X-RAY SPECTRAL FITS TO PSPC DATA FOR 3C 351

Model	Normalization[a]	α_E	N_H[b]	Second Parameter	χ^2(dof)
1. Power law	2.72 ± 0.17	0.47 ± 0.16	0.0039 ± 0.0027	...	61.1 (28)
2. Two power laws	$2.79^{+0.38}_{-0.20}$	$-0.04^{+0.34}_{-0.25}$	0.048 ± 0.030	$\alpha_2 > 3.1$	26.8 (26)
3. Partial covering	$13.9^{+4.4}_{-3.4}$	$2.12^{+0.42}_{-0.31}$	$2.00^{+0.69}_{-0.45}$	$F_C = 0.93^{+0.04}_{-0.05}$	26.2 (27)
4. Power law + edge	5.06 ± 0.67	$0.96^{+0.15}_{-0.10}$	0.68 ± 0.09	$E_0^c = 0.68^{+0.10}_{-0.20}$	33.1 (27)
5. Warm absorber	5.33 ± 0.70	0.5 (fixed)	$3.90^{+0.25}_{-0.60}$	$U = 0.126^{+0.006}_{-0.002}$	28.8 (28)
6. Warm absorber	$4.38^{+0.61}_{-0.50}$	0.6 (fixed)	$1.35^{+0.75}_{-0.30}$	$U = 0.155^{+0.035}_{-0.025}$	28.9 (28)
7. Warm absorber	$4.56^{+0.74}_{-0.64}$	0.7 (fixed)	$1.17^{+0.48}_{-0.33}$	$U = 0.140^{+0.030}_{-0.020}$	30.0 (28)
8. Warm absorber	5.22 ± 0.70	0.9 (fixed)	1.30 ± 0.45	$U = 0.175 \pm 0.040$	31.4 (28)
9. Warm absorber	5.41 ± 0.60	1.1 (fixed)	1.20 ± 0.30	$U = 0.216 \pm 0.075$	32.8 (28)

[a] At 1 keV, in units of 10^{-4} photons cm^{-2} s^{-1} keV^{-1}.
[b] In units of 10^{22} atoms cm^{-2}.
[c] In keV.

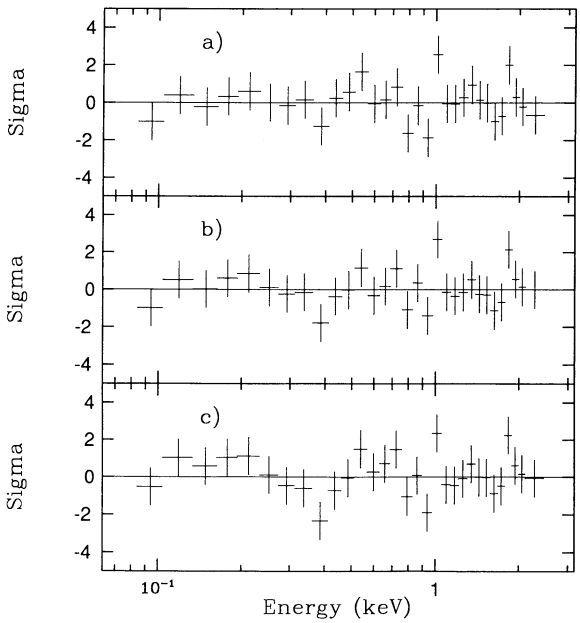

FIG. 3.—Residuals of fit to the spectrum of 3C 351 for (*a*) two-power-law model (soft component), (*b*) partial covering model, and (*c*) single power law plus absorption edge. Energies are in the observed frame.

AGNs, especially in lobe-dominated quasars (Shastri et al. 1993). Similar results were obtained parameterizing the soft excess as a blackbody (the temperature is again poorly constrained; $T \lesssim 0.08$ keV).

3.3. *Partial Covering*

The second modification is to make a partial covering model for the absorption law, so that only a fraction F_C of the source has this absorption applied to it. The Galactic absorption remains fixed at the Elvis et al. (1989) value. The results are again given in Table 1, and the residuals are shown in Figure 3*b*. The fit is again very good ($\chi_r^2 = 0.97$ for 27 dof), and the improvement in χ^2 with respect to the fit with model 1 is highly significant. The large N_H measured here, $(2.0^{+0.7}_{-0.4}) \times 10^{22}$ cm^{-2} (errors for three interesting parameters), takes into account the reduction of counts just below 1 keV seen in Figure 2, while the large number of counts observed between 0.1 and 0.6 keV is explained by the unobscured part of the source. The spectral index turns out now to be very steep, $\alpha_E = 2.12^{+0.42}_{-0.31}$. Quasars with such steep α_E have been observed in soft X-rays (e.g., PG 1211+143; Elvis et al. 1991a; see also Elvis, Wilkes, & McDowell 19901b for a review), but none of them have high intrinsic absorption detected as well.

3.4. *Warm Absorber*

Since these simple modifications gave unusual continuum slopes, we also investigated a third modification to the absorber in model 1, a "warm" absorber (Halpern 1984). This model leaves the ionization level of the absorber free to vary, as discussed by Krolik & Kallman (1984). When the ionization parameter, defined as

$$U = \frac{Q}{4\pi r^2 n_H c},$$

where Q is the total number of ionizing photons per second and n_H is the total number density of hydrogen, is very low, only the ground state and low-ionization states of the elements responsible for the absorption of X-rays are significantly populated, and the assumption of a completely neutral absorber is a good approximation of the actual situation. When the ionization parameter is high, most of the elements from H to O are completely ionized, and, at least in the 0.1–2.5 keV energy range, the assumption of no intrinsic absorption is a good one. When, however, not all the C, N, O, and Ne are completely ionized, they can give rise to significant absorption above $\sim$0.3 keV even if H and He are completely ionized. In particular, if He is completely ionized while the heavier elements are not, the gas is transparent below $\sim$0.3 keV and almost opaque above this energy. These warm absorbers give rise to edge structures in the transmitted spectrum, with the oxygen K-edges (0.54–0.87 keV) being the most prominent. Since a deficit between 0.6 and 0.9 keV is the largest feature in the residuals in Figure 2, models which include the possibility of an absorption edge are promising.

3.4.1. *Simple Power Law plus Edge*

As a first, simplified investigation we parameterize such a model assuming that the incident power law is absorbed by neutral gas with column density N_{H1} above an energy E_0, while below this energy it is absorbed only by the Galactic N_H. The results of this fit are again listed in Table 1 and are shown in Figure 3*c*. The χ_r^2 (1.23 for 27 dof) is again good, though marginally higher than in the previous two cases. The spectral index is $\alpha_E = 0.96^{+0.15}_{-0.10}$ (errors for three interesting parameters). This continuum slope is consistent with those of other lobe-dominated quasars (Shastri et al. 1993). The rest-frame energy E_0 of the edge is $0.68^{+0.1}_{-0.2}$ keV (errors for three interesting parameters). K-edges of ions of carbon, nitrogen, and oxygen are present in this energy interval (Band et al. 1990). The less conservative errors for just one interesting parameter reduce the confidence interval for the edge energy to 0.58–0.76 keV: only K-edges of N VII and O IV, O V, O VI, and O VII are present in this interval.

The "reasonable" spectral slope obtained with the above model suggests that a warm absorber may be appropriate. The above model is, however, not physical, and therefore the next step was the construction of a full warm absorber model using a photoionization code.

3.4.2. *Construction of a Physical Warm Absorber*

To construct a warm absorber model, only three ingredients are necessary: (*a*) the relative abundance of each ion of the elements responsible for the X-ray absorption in the studied energy range, (*b*) the elemental abundances, and (*c*) the cross-section for photoelectric absorption of each ion. The relative abundance of ions is a function of the number density of the gas, its column density, and the shape and intensity of the ionizing continuum. The photoionization code CLOUDY (version 80.06; Ferland 1991) was used to determine the relative abundances of all ions of H, He, C, N, O, Ne, Mg, Al, Si, S, Ar, Ca, and Fe (a total of 153 ions) for a grid of values of N_H (10^{21} cm$^{-2} \lesssim 10^{23}$ cm^{-2}), a series of simple ionizing continua, and a grid of values of the ionization parameter U (which is the dimensionless ratio between the number of ionizing photons and the gas density and therefore represents the normalization of the incident continuum, $0.04 \lesssim U \lesssim 0.25$). The abundances

relative to hydrogen of each element were fixed at the solar value (Grevesse & Anders 1989). The continuum was parameterized as a power law of slope α_E with low- and high-energy cutoffs. The resulting ion abundances are insensitive to the low-energy cutoff, provided that it is shortward of ~ 100 μm. In the following we fixed the low-energy cutoff at 10 μm, but the abundances do not differ qualitatively from those obtained with cutoffs from 100 μm to 912 Å. The ion abundances depend slightly on the position of the high-energy cutoff. We tried cutoffs at 50 keV and 5 MeV. The result is a slightly flatter emergent continuum when the cutoff is at 5 MeV ($\Delta\alpha_E \sim 0.2$). In the following we present the results fixing the high-energy cutoff at 5 MeV. The ion abundances do depend strongly on the slope of the incident continuum. We therefore computed them for a grid of values of α_E from 0.3 to 1.2. The abundances do not depend significantly on the volume density of the gas, provided that it is between 10^8 and 10^{11} cm^{-3}. We fix it at 10^9 cm^{-3}.

In conclusion, all the information obtained using CLOUDY is contained in a four-dimensional matrix [153 (ions) $\times$ N (values of α_E), $\times$ M (values of U) $\times$ L (values of N_H)]. We used $N = 10$, $M = 15$, and $L = 20$. This model of warm absorbers has therefore three free parameters: the slope of the ionizing continuum, α_E, the ionization parameter, U, and the gas column density, N_H.

At present there are no universally accepted values for the photoionization cross sections. The uncertainties are particularly large for the cross sections for removal of the outer electrons of atoms. To understand to what extent the uncertainty in the cross sections can affect the evaluation of the parameters of the warm absorber, we used two different sets of cross sections. The first was extracted from CLOUDY and consists of unpublished values by C. Mendoza (Ferland 1991). The second is a compilation by A. Fazzolari and G. C. Perola constructed by using the results of Reilman & Manson (1979), and by using the formulae of Band et al. (1990) to find the cross sections of each ion at energies greater than the K-edge. The positions of the K absorption edges are from Band et al. (1990); those of the L and M edges of neutral atoms are from Henke et al. (1982). All this information is contained in a two-dimensional matrix [479 (energies) $\times$ 153 (ions)].

3.4.3. *Fitting the Warm Absorber Model*

The opacity of the gas as a function of the energy and for each given value of α_E, U, and N_H is found by interpolating linearly over the matrix of the ion abundances and then multiplying the result of the matrix of the cross sections. The discrepancies between interpolated abundances and "true" ones (those found by running CLOUDY) are always smaller than 10%. In the following we present the results obtained using the CLOUDY cross sections and discuss the differences with those obtained using the Fazzolari and Perola cross sections.

Since nothing is known about the location of X-ray warm absorbers, and to limit as much as possible the number of free parameters, in the following analysis we adopted the simplest possible geometry, i.e., a plane-parallel geometry (with the thickness of the cloud much smaller than the distance between the cloud and the source of the X-ray continuum), where a single cloud completely and uniformly covers the continuum source. The "geometric" covering factor of the cloud (i.e., the fraction of the source along the line of sight covered by the source) is therefore unity, while the "radiative" covering factor (as defined by Ferland 1991, $f_c = \Omega/4\pi$) is very small and corresponds to an open geometry. The redshift of the warm absorber is fixed at 0.371. A further neutral absorber, of density fixed to the Elvis et al. (1989) Galactic value and redshift zero, covers the source.

The χ_r^2 obtained by fitting the warm absorber model to the data with all the parameters free is good, 1.06 for 27 dof, but the uncertainties on α_E, U, and N_H are large. This is because the moderate energy resolution of the PSPC and the complexity of the model produce a strong correlation between the three parameters. In other words, many models with different values of α_E, N_H, and U are able to reproduce the observed spectrum. In particular, the χ^2 is rather insensitive to the value of α_E. We therefore repeated the fit by fixing α_E at a set of values of α_E spanning the range commonly observed in quasar X-ray spectra (Wilkes & Elvis 1987; Williams et al. 1992), namely, 0.5, 0.6, 0.7, 0.9, and 1.1. The χ^2 are always very good. The results of the series of fits are given in Table 1, with errors for two interesting parameters, and the case of $\alpha_E = 0.9$ is shown in Figure 4*a*. In Figure 4*b* the transmitted continuum corresponding to this case is shown. The prominent absorption edge is due to O VII at 0.74 keV. The low-energy absorption is due to residual He opacity (in this model the relative abundances of He and He^+ are $\sim 2 \times 10^{-7}$ and 0.01, respectively). The 68%, 90%, and 99% contours of χ^2 as a function of U and N_H for the fits with the first four values of α_E are shown in Figure 5 (the contours for the fit with $\alpha_E = 1.1$ are similar to those for the fit with $\alpha_E = 0.9$ but centered at $U = 0.22$). The contours look quite different in the four cases, and the behavior of warm absorber models as U and N_H are changed appears quite complex. We have looked at these dependencies in some detail and, since they have not been widely discussed in the literature, we show how they can be understood in a reasonably intuitive manner in the Appendix.

The results obtained using the Fazzolari and Perola cross sections are similar concerning the χ^2, but the best-fit values of U and N_H are shifted systematically by $\sim 20\%$ toward lower values. This is due to the fact that the total cross section computed with the Fazzolari and Perola compilation is generally about 50% greater than the CLOUDY total cross sections in the keV region. Elsewhere the two total cross sections are generally within 15%–20% of each other.

4. DISCUSSION

The *ROSAT* PSPC observation has revealed that the 0.1–2.4 keV spectrum of 3C 351 is complex and cannot be represented by a simple absorbed power law. As discussed in the previous section, three different modifications of the simple power-law model are able to reproduce this complex spectrum within the limited energy resolution of the PSPC (about 0.5 keV at 1 keV). Each of the models can explain the results obtained with the IPC, where the source was found with a flat spectrum (Elvis et al. 1993) during a long (live time of 33,100 s) observation. In all three models the observed spectrum is flat between ~ 0.6 and 2.5 keV and steepens significantly toward lower energies, while the intrinsic, emitted spectra differ strongly.

Two of the models, however, require unusual conditions: in the two–power-law model the spectral index of the harder power law is unusually flat for an AGN, especially for a lobe-dominated quasar (Shastri et al. 1993); in the partial covering model the spectral index is very steep, $\alpha_E \sim 2$, similar to that measured in an extreme object like PG 1211+143 (Elvis et al.

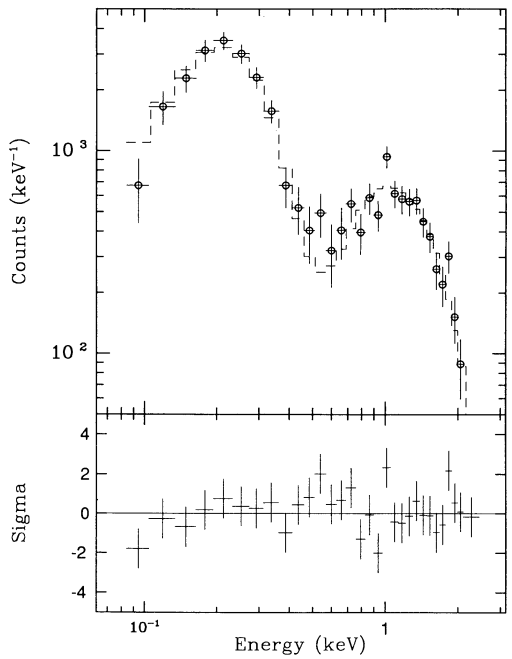

FIG. 4*a*

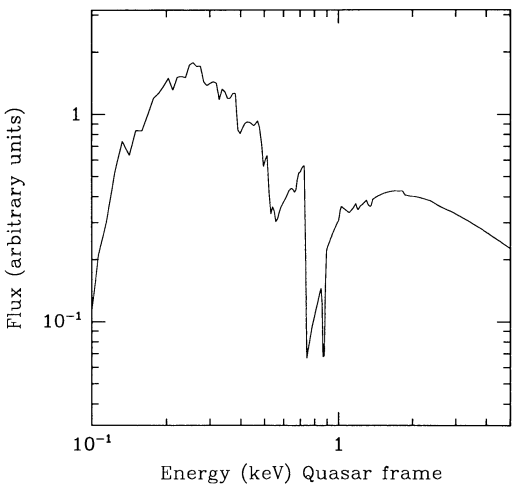

FIG. 4*b*

FIG. 4.—Warm absorber model spectral fit to the spectrum of 3C 351 (α_E fixed at 0.9). (*b*) The best-fitting transmitted spectrum. The deep edge at $\sim$0.74 keV is due to O VII. Energies are in the quasar frame.

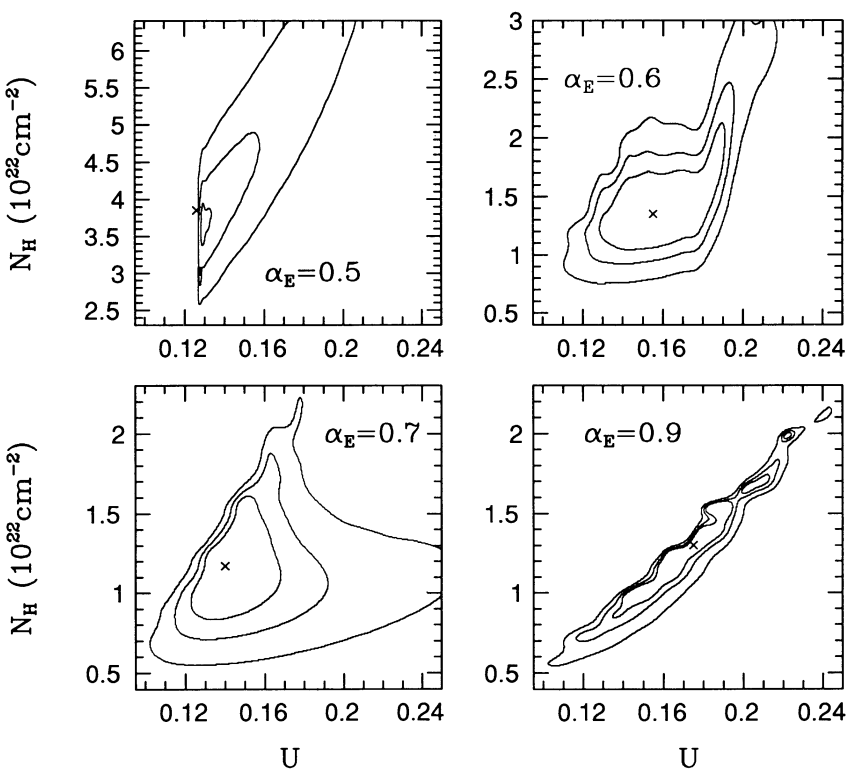

FIG. 5.—*U*-N_H 68%, 90%, and 99% confidence contours for the warm absorber model for α_E = 0.5, 0.6, 0.7, and 0.9

1991a). The partial covering model also requires a column density of $\sim 10^{22}$ cm^{-2}, covering 90% of the source to reduce the counts below 1 keV. None of the known "soft X-ray quasars" (Elvis et al. 1991b) has an intrinsic column density of this magnitude. On the other hand, the warm absorber model provides a good fit for the values of α_E spanning the range commonly observed in quasar X-ray spectra (Wilkes & Elvis 1987; Williams et al. 1992).

Unlike the warm absorber model, the two–power-law model and the partial covering model have been extensively used and discussed in previous studies of AGN X-ray spectra. While not excluding these two models, below we will therefore discuss on a deeper level of detail the implications of the warm absorber model. First we discuss the implications of this observation for the "X-ray quietness" issue.

4.1. *X-Ray Quietness*

Our observation of 3C 351 allows strong constraints to be placed on the origin of X-ray quietness. In the past, measurements of X-ray/optical ratios have been compromised by the possibility of variability between the nonsimultaneous multiwavelength observations. In the optical 3C 351 is quite bright ($B \approx 15.9$) and mildly variable. Angione (1973) and Grandi & Tifft (1974) report variations of a factor ~ 2 on time scales of 5–10 yr. To avoid the problem of variability, we observed 3C 351 in the optical nearly simultaneously with the *ROSAT* observation. The details of the optical observations, performed with the MMT, will be presented elsewhere (Mathur et al. 1993). By a fortunate coincidence, 3C 351 was also observed in the UV by the *Hubble Space Telescope* (*HST*) just 1 week before *ROSAT* (Bahcall et al. 1993). From these nearly simultaneous optical and UV observations, it is possible to estimate the 2500 Å source flux during 1991 October to be 4.1×10^{-15} ergs cm^{-2} s^{-1} Å^{-1}. the value of α_{OX} can therefore be estimated for the four models described in the previous section (see Table 2, which also contains the unabsorbed 0.1–2.45 keV flux for each model).

We see that in the simple power-law model and in the partial covering model α_{OX} is ~ 1.6, consistent with the finding of Tananbaum et al. (1986), while it is significantly lower both in the two–power-law model (1.52) and in the warm absorber model (1.54). the mean α_{OX} found by Tananbaum et al. (1983) by analyzing a complete sample of 33 3CR quasars is 1.37, with a standard deviation of 0.15. For each quasar α_{OX} was computed assuming $\alpha_E = 0.5$ and Galactic absorption. The peculiar flatness of the spectrum of 3C 351 in the "keV" region (either because intrinsically so or because of intrinsic absorption) can explain about 35% (two–power-law model) or 25% (warm absorber model) of the difference between the mean α_{OX} and the 3C 351 α_{OX} when the Tananbaum et al. (1983) prescription is adopted.

Since our measurement of α_{OX} for 3C 351 was obtained with quasi-simultaneous optical, UV, and X-ray observations, we can use it to rule out several possibilities for explaining X-ray quietness. Extreme variability is not allowed. Absorption is already corrected for in Table 2, and so, while it can reduce the spread in α_{OX} somewhat, it does not explain the entire range. Extremely steep or flat intrinsic spectra are possible if the partial covering or soft excess models are correct. The warm absorber model suggests, although we have only one case, that the α_{OX} distribution for quasars does have a real width, which is due to a range of intrinsic X-ray normalizations relative to the optical of sources with similar spectra. This intrinsic width, however, is probably somewhat smaller than that estimated by Tananbaum et al. (1983), owing to a contribution from absorption.

4.2. *Warm Absorber Models*

Warm absorbers have been invoked previously to explain the X-ray spectra of AGNs and quasars: MR 2251−178 (Halpern 1984; Pan et al. 1990), MCG −6-30-15 (Nandra, Pounds, & Stewart 1990; Nandra & Pounds 1992), NGC 4051 (Fiore et al. 1992), and NGC 6814 (Turner et al. 1992). For MCG −6-30-15 the evidence for a warm absorber comes from the detection of an edgelike structure in a *ROSAT* spectrum (Nandra & Pounds 1992). These authors fitted to the data a simple power law plus edge model similar to that discussed in § 3.4.1. They found a somewhat higher edge energy (0.825 ± 0.017 keV), suggesting a higher value for the ionization parameter than in the present case. Apart from MCG −6-30-15 and 3C 351, evidence for warm absorbers is mostly less direct. This is because of insufficient energy resolution below 1 keV where most of the absorption edges are located. MR 2251−178 is, however, particularly interesting because its X-ray luminosity is similar to that of 3C 351 and is the highest among the above sources. The variable absorption in MR 2251−178 correlates with the X-ray luminosity as predicted by warm absorber models, since the opacity of the absorber is critically balanced against the incoming ionizing continuum and changes strongly in response to relatively small variations in that continuum.

The interpretation of the complex soft X-ray spectrum of 3C 351 in terms of an ionized absorber is not unique, because of the limited energy resolution of the PSPC. Observations of the source above 2 keV with good signal-to-noise ratio, as it will be possible to perform with *Asuka*, would constrain the X-ray slope and therefore would discriminate among the three models discussed in the previous section.

TABLE 2

3C 351: X-RAY FLUXES AND LUMINOSITIES

Model	f_{PSPC}[a] (0.1–2.45 keV)	f_{IPC}[a] (0.5–4.5 keV)	L[b] (0.1–2.45 keV)	α_{OX}
1. Power law	$1.08^{+0.13}_{-0.10}$	$1.25^{+0.15}_{-0.12}$	$1.11^{+0.10}_{-0.08}$	1.59
2. Two power laws	>2.4	>2.3	>1.3	1.52
3. Partial covering	25^{+41}_{-13}	$3.9^{+1.4}_{-0.9}$	16^{+19}_{-7}	1.60
8. Warm absorber ($\alpha_E = 0.9$)	2.5 ± 0.4	1.5 ± 0.3	2.0 ± 0.5	1.54

[a] Unabsorbed flux in units of 10^{-12} ergs cm^{-2} s^{-1}.

[b] In units of 10^{45} ergs s^{-1} (assuming $H_0 = 50$ km s^{-1} Mpc^{-1} and $q_0 = 0, z = 0.37$).

Another crucial test for the warm absorber model would be observations of large amplitude variations (a factor of 2 or more), since this model makes stringent predictions about the changes in soft X-ray opacity at different energies in response to variations in the ionizing continuum. Unfortunately, during the 3 days of the *ROSAT* observation the source showed no variations larger than $\sim 40\%$. Factor of 2 variations are present in the 0.16–3.5 keV light curve of the 12 IPC observations (Cordova et al. 1992; see their Fig. 6 and Table 3). The amplitude of the variations seems to be different in their three bands (0.16–0.56 keV, 0.56–1.08 keV, and 1.08–3.5 keV), thus suggesting the existence of spectral variability, but no clear correlations exist among the three bands. The statistics are, however, so poor that no definite conclusion can be drawn. Future observations can decisively test the warm absorber model in this quasar.

The confidence intervals for U and $N_{\rm H}$ obtained in § 3.4.3 for normal values of the spectral index are reasonably narrow. In particular, U is limited to the range 0.1–0.2, with the lower limit being particularly stringent, and $N_{\rm H}$ to the range (1–5) $\times 10^{22}$ cm^{-2}. These values depend, however, on the particular shape adopted for the ionizing continuum. Changing the shape would result in a modification of the best-fit U, since the ionization parameter can be considered as the normalization of the 0.0136–5000 keV ionizing continuum. Furthermore, as pointed out recently by Netzer (1993), the ionized gas will emit in the X-ray band both lines and continua, and will reflect towards the observer part of the incident continuum. These components might reduce the depth of the oxygen edges, and therefore the best-fit values for the ionization parameter and column density obtained with a model which does not include such features would be lower than the actual U and $N_{\rm H}$.

The reduction of the depth of the oxygen edges depends on the intensity of the emitted and reflected radiation in the 0.5–1 keV region, which in turn depends on the geometry of the gas (i.e., on the covering factor) and on the column density and the ionization parameter. In particular, the reflected component varies greatly with f_c, being zero when the covering factor is zero (as for a single cloud along the line of sight, i.e., the warm absorber model in § 3.4.3) and reaching a maximum when the covering factor is 0.5 (Netzer 1993). The intensity of the reflected component varies also with the energy, and it has a broad minimum around the energies of the O VII and O VIII edges (Netzer 1993). Therefore, even for small but nonzero covering factors, reflection should not weaken the oxygen edges significantly. Also, the intensity of the continuum and line emission depends greatly on the geometry adopted. The intensity is smallest when a single cloud of dimension larger than the source of the ionizing radiation completely covers the line of sight. The intensity of the continuum and line emission varies greatly with U and $N_{\rm H}$, increasing rapidly toward large $N_{\rm H}$ (of the order of 10^{23} cm^{-2}) and large U ($U \gtrsim 1$). For the best-fit value obtained for U and $N_{\rm H}$ in § 3.4.3, the strongest emission lines in the *ROSAT* band are at 0.574 keV (O VII) and 0.654 keV (O VIII and the recombination line from fully stripped ions). The detection of these individual lines with instruments having good energy resolution, such as the CCDs that will be on board *Asuka*, JET-X and XMM (although it is not clear whether these CCDs will have enough sensitivity at these low energies), and the calorimeter that will be on board *AXAF-S* would permit constraints to be placed on the geometry of the gas. Furthermore, since for a given value of $N_{\rm H}$ the relative intensity of these lines changes strongly as a function of U, measuring their ratio would provide a detailed diagnostic of the warm gas.

Keeping in mind the limitations discussed above on the constraints obtained in § 3.4.3 on U and $N_{\rm H}$, we can tentatively estimate the physical thickness of the warm absorber and its distance from the central source, with only the volume density as a free parameter. The geometric depth of the region containing the ionized gas is

$$\Delta R = 10^{13}\left(\frac{N_{\rm H}}{10^{22}\ {\rm cm}^{-2}}\right)\left(\frac{n_{\rm H}}{10^{9}\ {\rm cm}^{-3}}\right)^{-1}\ {\rm cm}\ ,$$

where $n_{\rm H}$ is the total number density of hydrogen. From the definition of ionization parameter, and by using the best-fit parameters for the case $\alpha_E = 0.9$ to find $Q \approx 3 \times 10^{55}$ photons s^{-1}, it follows that the distance of the gas from the source of the continuum, r, is

$$r = 9 \times 10^{17}\left(\frac{U}{0.1}\right)^{-1/2}\left(\frac{n_{\rm H}}{10^{9}\ {\rm cm}^{-3}}\right)^{-1/2}\ {\rm cm}\ ,$$

assuming isotropic emission. This is similar in size to the broad-line region of quasars of this luminosity, and much larger than expected accretion disk dimensions (for $10^8 \lesssim n_{\rm H} \lesssim 10^{11}$ cm^{-3}). Such a large dimension for the region containing the warm gas is, however, inconsistent with the assumption of a simple power-law ionizing continuum of slope $\lesssim 1$, since most of the optical-UV radiation should be generated well within the central parsec, and the $\alpha_{\rm OX}$ of this quasar is in the range 1.5–1.6. Since the ionization structure of oxygen is mainly determined by the number of ionizing photons around 0.5 keV, the inclusion in the ionizing continuum of a steep optical-UV component (in addition to the X-ray power law), should change only the normalization of the ionizing continuum (i.e., the ionization parameter). The value of U which gives rise to similar relative abundances of oxygen ions would then be higher than in the simple power-law case. In fact, assuming a photoionizing continuum consisting of a broken power law, with an X-ray slope of unity and a UV-soft X-ray slope of 4 again produces a good fit while giving U in the range 1–2.5 (Mathur et al. 1993).

The association of the warm absorber with the BLR could also be tested for consistency using the predicted intensities for the optical and UV emission lines that must arise from the absorbing material. The detailed investigation of a self-consistent warm absorber model able to explain the broad-band optical-UV and X-ray continuum and line emission is, however, beyond the scope of this paper and will be part of a follow-up paper (Mathur et al. 1993).

5. CONCLUSIONS

The quasar 3C 351 has been found to have a complex soft X-ray spectrum. Warm absorber, partial covering, and soft excess models can all produce acceptable fits, although only the warm absorber model gives a good χ^2 for typical values of the high-energy continuum slope.

Whichever model is correct, this observation of 3C 351 limits the possible causes for "X-ray quietness." Quasi-simultaneous X-ray, optical, and ultraviolet (*HST*) observations of 3C 351 make it highly unlikely that variability is the main cause of the wide range of $\alpha_{\rm OX}$ observed in quasars. Spectral fits that allow for intervening absorption increase the intrinsic emitted X-ray flux of 3C 351 by only a minor part of the difference in $\alpha_{\rm OX}$ ($\approx 25\%$). If a warm absorber model applies, then the $\alpha_{\rm OX}$ of 3C 351 originates not in an unusual X-ray spectrum but in a reduced normalization relative to the

optical indicating efficiency of X-ray production or a beamed component as the potential causes of different levels of X-ray emission. For the other models, extremely steep or extremely hard continua also contribute to the X-ray quietness of 3C 351.

If a warm absorber model is assumed, then the strongest absorption edge feature lies in the range 0.58–0.76 keV (1 σ, one interesting parameter), implying O IV–O VII as the most likely absorbing ions. The ionization parameter and column density of the absorber are constrained to 0.1–0.2 and (1–5) $\times 10^{22}$ atoms cm^{-2}, respectively (for a power-law ionizing continuum). Factor of 2 variability of the ionizing continuum should result in strong changes in the soft X-ray opacity of the warm absorber and so would provide a strong test for this model. Furthermore, observations of the source in different states of intensity would permit a constraint on the spectral index of the radiation incident on the absorbing gas (see the Appendix).

As noted in § 1, radio observations suggest that 3C 351 is likely to be an almost edge-on quasar (e.g., Leahy & Perley 1991). Also, Eracleous & Halpern (1992) claim a double-peaked Hα emission-line profile in this quasar. Double-peaked profiles are a signature of relativistic accretion disks not viewed face-on. This is consistent with the absence of any beamed component. Also, quite possibly our line of sight passes through gas at the edge of an "obscuring torus" suggested in unified models. 3C 351 may provide a new tool for investigating conditions in this hypothesized torus, via variability monitoring or higher resolution spectra.

The PSPC energy band is particularly good to search for warm absorbers which would reduce the 0.5–1 keV flux without totally removing photons in the 0.25 keV region, as can be seen from the color diagram in Figure 7 (see the Appendix). Since the region occupied by the warm absorber model in this diagram is well separated from the region occupied by simple power-law plus cold absorption models (unless the column density is much lower than the Galactic one), such diagrams will be useful for selecting candidate warm absorbers. By using these diagrams, it will be possible to search efficiently for warm absorbers in large samples, for any source with at least 400 counts.

We would like to thank G. Ferland for providing us with the latest version of his photoionization code CLOUDY, and A. Fazzolari and G. C. Perola for providing us with their compilation of atomic cross sections and for many stimulating discussions. We thank also M. Birkinshaw for a careful reading of the manuscript and for his many comments. This work was supported by NASA grants NAGW-2201 (LTSARP), NAG 5-1872, and NAG 5-1536 (*ROSAT*), NASA contracts NAS 8-39073 (*AXAF* Science Center), NAS 5-30934 (ROSAT Data Center), and NAS 5-30751 (*HEAO 2*).

APPENDIX

THE BEHAVIOR OF WARM ABSORBER MODELS

The behavior of warm absorber models as α_E, U, and N_H are changed is complex. This shows up clearly in the χ^2 contours in Figure 5, which look quite different in ways that appear confusing. For $\alpha_E = 0.9$, U and N_H are strongly correlated and the gradients in the χ^2 surface on both sides of this correlation are very steep (for a given N_H, U is tightly constrained). For $\alpha_E = 0.7$ only the gradients going toward high N_H and low U are steep. For $\alpha_E = 0.6$ the gradients are rather shallow going toward both low and high U. For $\alpha_E = 0.5$ the gradients are again very steep going towards low U.

This apparently confusing situation can be understood more readily from Figure 6, in which we show the transmitted spectra for $\alpha_E = 0.5$, 0.6, and 0.9 and for three values of U. It is instructive to compare the changes at 0.25 and 1 keV, where the effects of helium and oxygen ionization, respectively, are dominant. For $\alpha_E = 0.9$ (and $N_H = 1.2 \times 10^{22}$ cm^{-2}) (*right-hand panel*), changing U through 0.12 and 0.18 produces a change in the opacity and so affects the transmitted spectrum mainly below 0.3 keV. The most prominent edge is that of O VII at 0.74 keV (except for $U = 0.18$), and it is always deep enough to reproduce adequately the data around that energy. For $U \lesssim 0.14$ a large fraction of helium and carbon atoms are not completely ionized and give rise to a low-energy cutoff too strong to be compatible with the data. For $\alpha_E = 0.6$ (and $N_H = 1.2 \times 10^{22}$ cm^{-2}) (*center panel*), changing U through the same interval produces changes of comparable amplitude both at 0.25 keV and at 1 keV. The most prominent edge is that of O VII. For $\alpha_E = 0.5$ (and $N_H = 3.5 \times 10^{22}$ cm^{-2}) (*left panel*) the changes at both 0.25 and 1 keV are very large. The most prominent edge is now that of O VIII at 0.87 keV. For $U \gtrsim 0.14$ most helium and carbon atoms are completely ionized, as are a large fraction of oxygen atoms, and the O VIII edge is not deep enough to fit the data. When $U \lesssim 0.125$, helium atoms are mostly neutral and contribute heavily to the absorption, so the spectrum is strongly cut off below ~ 0.3 keV.

The gradients in the χ^2 surfaces are steep going toward low U because the transmission at 0.25 keV saturates at unity as U increases well before the transmission at 1 keV and because χ^2 is more sensitive to the strength of the low-energy cutoff than to the depth of the ~ 0.7–0.9 keV edge.

The amplitude of the changes at 1 keV increases going toward flatter α_E as oxygen ionization grows rapidly. The amplitude of the changes at 0.25 keV decrease going from $\alpha_E = 0.9$ to $\alpha_E = 0.6$, and then increases again. For $\alpha_E = 0.6$ the U-N_H allowed region is broader because, while the O VII is always reasonably deep, the changes at 0.25 keV are smaller than for $\alpha_E = 0.7$ and 0.9.

Inspection of Figure 6 identifies two observationally convenient energy intervals, one centered around 0.25 keV and the other at 1 keV (in the quasar frame), to which our modeling is particularly sensitive. They correspond, as noted above, to energies at which the opacity of helium (and carbon) and oxygen, respectively, dominate. The level of agreement of a given model with the data is thus largely determined by the ratio between the flux at 0.25 and 1 keV. In Figure 7 we plot the ratio between the expected PSPC counts in the intervals 1.2–2.4 and 0.6–1.0 keV as a function of the ratio between the counts in the intervals 0.2–0.4 and 0.6–1.0 keV (0.27–0.55, 0.82–1.37, and 1.64–3.29 keV in the 3C 351 frame) for three values of α_E and U in the range 0.1–0.2. The point with error bars represents the ratios actually measured in the case of 3C 351 with the 1 σ uncertainty. The shape of the curves varies with α_E, while increasing N_H simply moves the $\alpha_E = 0.7$ curve toward lower values of the 0.2–0.4 keV/0.6–1.0 keV ratio and higher values of

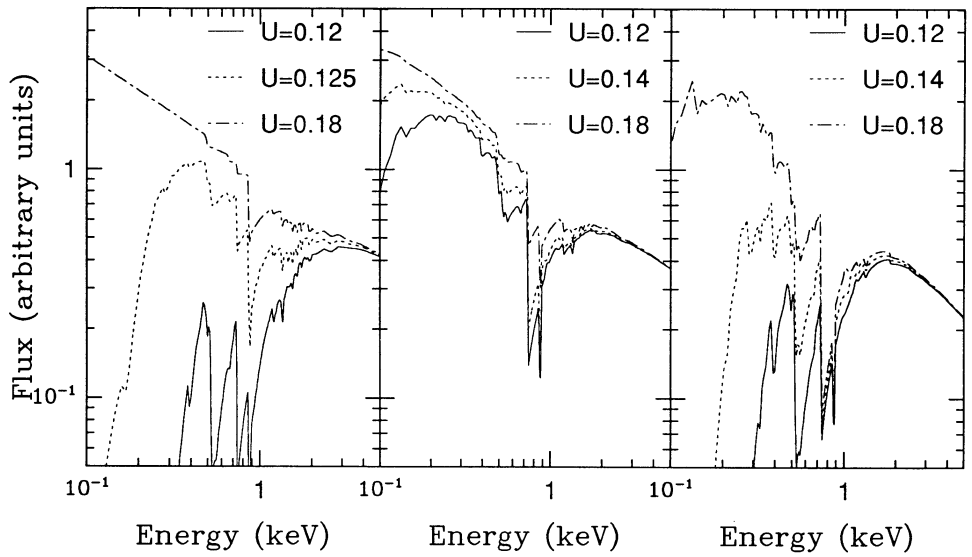

FIG. 6.—Transmitted spectra for (*left*) $\alpha_E = 0.5$, $N_H = 3.5 \times 10^{22}$ cm^{-2}, (*center*) $\alpha_E = 0.6$, $N_H = 1.2 \times 10^{22}$ cm^{-2}, (*right*) $\alpha_E = 0.9$, $N_H = 1.2 \times 10^{22}$ cm^{-2}, and for three values of the ionization parameter.

the 1.2–2.4 keV/0.6–1.0 keV ratio. This suggests that observations of the source in different states of intensity (and therefore with a different U) would permit a constraint on the spectral index of the radiation incident on the absorbing gas.

Color diagrams like that in Figure 7 could also be a simple and useful tool to search for warm absorbers in AGNs in the PSPC energy band. In particular, absorbers in which most helium atoms are completely ionized, while oxygen atoms are not, produce PSPC spectra significantly flatter in the keV region than at 0.25 keV. In a color-color diagram these models occupy a well-defined region. As an example, the small stars in Figure 7 represent the ratios computed from model 1 with absorption fixed at the Galactic value and $\alpha_E = 2$, 1.5, 1, and 0.5 (both ratios increase as the spectral index flattens). Increasing (decreasing) N_H moves the points toward lower (higher) ratios. The big star represents the ratios computed from the best-fitting model 1 (with $\alpha = 0.47$,

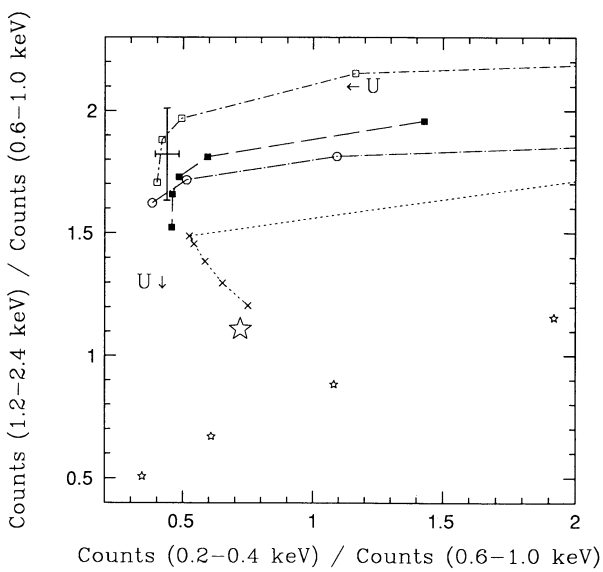

FIG. 7.—Ratio of the counts in the energy intervals 1.2–2.4 keV and 0.6–1.0 keV plotted as a function of the ratio in the intervals 0.2–0.4 keV and 0.6–1.0 keV for $\alpha_E = 0.5$, $N_H = 1.2 \times 10^{22}$ cm^{-2} (*crosses*); $\alpha_E = 0.7$, $N_H = 1.2 \times 10^{22}$ cm^{-2} (*filled squares*); $\alpha_E = 0.7$, $N_H = 1.5 \times 10^{22}$ cm^{-2} (*open squares*); and $\alpha_E = 0.9$, $N_H = 1.2 \times 10^{22}$ cm^{-2} (*open circles*). In all cases U is varied between 0.1 and 0.2. The point with error bars represents the ratios measured from the 3C 351 spectrum with the 1 σ uncertainty (no systematic error has been added here to the statistical error in each channel). The big star represents the ratios computed from the best-fitting model 1 in Table 1. The small stars represent the ratios computed from model 1 with absorption fixed at the Galactic value of 2.26×10^{20} cm^{-2} and $\alpha_E = 2$, 1.5, 1, and 0.5 (both ratios increase as the spectral index flattens). Increasing (decreasing) N_H moves the points toward lower (higher) ratios.

$N_H = 3.9 \times 10^{19}$ cm^{-2}, much lower than the Galactic value along the line of sight): only for this extremely low value of the absorbing column does the point representing model 1 fall near some of the warm absorber models. It is, however, 6.2 and 3.7 σ from the corresponding ratios measured in the case of 3C 351.

REFERENCES

Abramowitz, M., & Stegun, I. A. 1964, Handbook of Mathematical Functions (New York: Dover)
Angione, R. J. 1973, AJ, 78, 353
Avni, Y., & Tananbaum, H. 1986, ApJ, 305, 83
Bahcall, J., et al. 1993, ApJS, 87, 1
Band, I. M., TrzhaskovsKaja, M. B., Verner, D. A., & Yakovlev, D. G. 1990, A&A, 237, 267
Barthel, P. D. 1989, ApJ, 336, 606
Blandford, R. D., & Königl, A. 1979, ApJ, 232, 34
Cordova, F. a., Kartje, J. F., Thompson, R. J., Mason, K. O., Puchnarewicz, E. M., & Harnden, F. R. 1992, ApJS, 81, 661
Elvis, M., & Fabbiano, G. 1984, ApJ, 280, 91
Elvis, M., Giommi, P., Wilkes, B. J., & McDowell, J. C. 1991a, ApJ, 378, 537
Elvis, M., Lockman, F. J., & Wilkes, B. J. 1989, AJ, 97, 777
Elvis, M., Wilkes, B. J., & McDowell, J. C. 1991b, in EUV Astronomy, ed. R. Malina & S. Bowyer (New York: Pergamon), 238
Elvis, M., et al. 1993, in preparation
Eracleous, M., & Halpern, J. P. 1992, in AIP Conf. Proc. 254, Testing the AGN Paradigm, ed. S. S. Holt, S. G. Neff, & C. M. Urr (New York: AIP), 216
Ferland, G. 1991, Hazy, OSU Astron. Dept. Internal Rep.
Fiore, F., Perola, G. C., Matsuoka, M., Yamauchi, M., & Piro, L. 1992, A&A, 262, 37
Gioia, I. M., Maccacaro, T., Schild, R. E., Wolter, A., Stocke, J. T., Morris, S. L., & Henry, J. P. 1990, ApJS, 72, 567
Grandi, S., & Tifft, W. G. 1974, PASP, 86, 873
Grevesse, N., & Anders, E. 1989, in AIP Conf. Proc. 183, Cosmic Abundances of Matter, ed. C. J. Waddington (New York: AIP)
Halpern, J. P. 1984, ApJ, 281, 90
Henke, B. L., Lee, P., Tanaka, T. J., Shimabukuro, R. L., & Fujikawa, B. K. 1982, Atomic Data Nucl. Data Tables, Vol. 27, No. 1
Kellerman, K. I., Sramek, R., Schmidt, M., Shaffer, D. B., & Green, R. 1989, AJ, 98, 1195
Krolik, J. H., & Kallman, T. R. 1984, ApJ, 286, 366
Lampton, M., Margon, B., & Bowyer, S. 1976, ApJ, 208, 177
Leahy, J. P., & Perley, R. A. 1991, AJ, 102, 737
Makino, F., et al. 1989, ApJ, 347, L9
Marscher, A. P. 1988, ApJ, 334, 552
Mathur, S., Fiore, F., Elvis, M., Wilkes, B. J., & McDowell, J. C. 1993, in preparation
Morrison, R., & McCammon, D. A. 1983, ApJ, 270, 119
Nandra, K., & Pounds, K. A. 1992, Nature, 356, 215
Nandra, K., Pounds, K. A., & Stewart, G. C. 1990, MNRAS, 242, 660
Netzer, H. 1993, ApJ, 411, 594
Orr, M. J. L., & Browne, I. W. A. 1982, MNRAS, 200, 1067
Pan, H. C., Stewart, G. C., & Pounds, K. A. 1990, MNRAS, 242, 177
Pfefferman, E., et al. 1987, Proc SPIE, 733, 519
Raymond, J. C., & Smith, B. W. 1977, ApJS, 35, 419
Reilman, R. F., & Manson, S. T. 1979, ApJS, 40, 815
Shastri, P., Wilkes, B. J., Elvis, M., & McDowell, J. C. 1993, ApJ, 410, 29
Tananbaum, H., Avni, Y., Green, R. F., Schmidt, M., & Zamorani, G. 1986, ApJ, 305, 57
Tananbaum, H., Wardle, J. F. C., Zamorani, G., & Avni, Y. 1983, ApJ, 268, 60
Trümper, J. 1983, Adv. Space Res., 2 (No. 4), 241
Turner, T. J., Done, C., Mushotzky, R., Madejski, G., & Kunieda, H. 1992, ApJ, 391, 102
Turner, T. J., & George, I. M. 1992, Office for Guest Investigator Programs Calibration Memo
Turner, T. J., Weaver, K. A., Mushotzky, R. F., Holt, S. S., & Madejsky, G. M. 1991, ApJ, 381, 85
Véron-Cetty, M.-P., & Véron, P. 1991, ESO Sci. Rep. No. 10
Wilkes, B. J., & Elvis, M. 1987, ApJ, 323, 243
Wilkes, B. J., et al. 1993, in preparation
Williams, O. R., et al. 1992, ApJ, 389, 157
Zamorani, G., et al. 1981, ApJ, 245, 357